Author's version
Published in: Transactions on Robotics, Vol 32, Issue 6, December 2016
DOI: 10.1109/TRO.2016.2604496

Reducing the energy consumption of robots using the Bi-directional Clutched Parallel Elastic Actuator

Michiel Plooij†, Martijn Wisse and Heike Vallery
Delft University of Technology

***Abstract*—Parallel elastic actuators (PEAs) have shown the ability to reduce the energy consumption of robots. However, regular PEAs do not allow to freely choose at which instant or configuration to store or release energy. This paper introduces the concept and the design of the Bi-directional Clutched Parallel Elastic Actuator (BIC-PEA), which reduces the energy consumption of robots by loading and unloading a parallel spring with controlled timing and direction. The concept of the BIC-PEA consists of a spring that is mounted between the two outgoing axes of a differential mechanism. Those axes can also be locked to the ground by two locking mechanisms. At any position, the BIC-PEA can store the kinetic energy of a joint in the spring such that the joint is decelerated to zero velocity. The spring energy can then be released, accelerating the joint in any desired direction. Such functionality is suitable for robots that perform rest-to-rest motions, such as pick-and-place robots or intermittently moving belts. The main body of our prototype weighs 202 g and fits in a cylinder with a length of 51 mm and a diameter of 45 mm. This excludes the size and weight of the non-optimized clutches, which would approximately triple the total volume and weight. In the results, we also omit the energy consumption of the clutches. The BIC-PEA can store 0.77 J and has a peak torque of 1.5 Nm. Simulations show that the energy consumption of our one DOF setup can be reduced by 73 %. In hardware experiments, we reached peak reductions of 65 % and a reduction of 53 % in a realistic task, which is larger than all other concepts with the same functionality.**

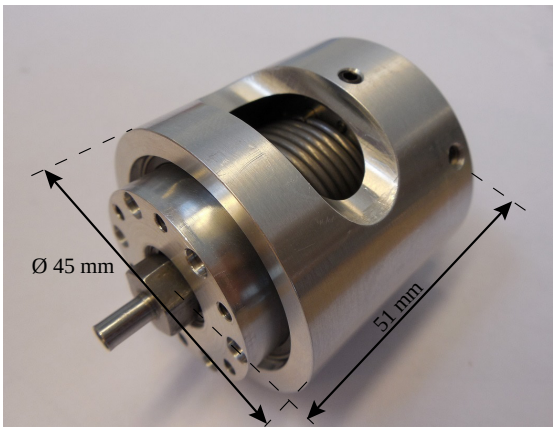

Figure 1. A photograph of the BIC-PEA. It weighs 202 g and fits in a cylinder with a length of 51 mm and a diameter of 45 mm.

I. Introduction

Energy consumption of robots is an increasingly important performance criterion. For instance, in the automotive industry, up to 50 % of the energy required to produce a car, is consumed by robots [1]. In mobile systems that rely on batteries, a low energy consumption is critical for a long operating time and low weight. Examples include domestic robots [2], walking robots [3], exoskeletons [4, 5] and prostheses [6–8]. One of the most promising approaches to reduce the energy consumption is recapturing negative work. Two main approaches are commonly applied in robots: generators and potential energy storage devices such as springs.

Electric motors can function as generators and transfer negative mechanical work into electrical energy to charge the battery. This has the advantage that the energy exchange between the energy storage and the joints is fully controllable. However, electrical motors suffer from copper losses, which decreases the efficiency of the energy recapture. Moreover, such motors often require gearboxes with large gearbox ratios that also increase the joint friction and thus increase the energy consumption of the robot. The efficiency of the energy recapture is further reduced by batteries that do not have a 100 % efficiency. A state-of-the-art robot that uses motors as generators is the Cheetah robot [9]. Seok et al. report an efficiency of energy recapture from joint to battery in the Cheetah robot of 63 %. Since their efficiency is mainly determined by copper losses, we can assume that the efficiency from the battery to the joint is approximately the same, meaning that the total efficiency is only 40 %.

Storing energy in the form of potential energy is potentially more energy efficient. Actuators that exploit an elastic energy buffer are called Elastic Actuators (EAs). Springs typically exhibit a hysteresis of 1-5 % and thus high efficiencies seem achievable in EAs. In general, EAs can be split into Parallel Elastic Actuators (PEAs) [10–20] and Series Elastic Actuators (SEAs) [21–25]. In the latter category, many researchers have designed SEAs with variable stiffnesses [23–25] and clutches [26, 27]. However, the ability of SEAs to reduce the energy consumption is limited, because the force on the joint also passes through the motor. An interesting new development in this field is the Series Parallel Elastic Actuator (SPEA) [19, 28]. Current SPEAs can be seen as SEAs with a reduced load on the motor. However, their designs are relatively large and difficult to miniaturize.

EAs in parallel with the motor have a larger potential to reduce the energy consumption, because the EAs take over part of the task from the motor. With a regular parallel spring,

† Corresponding author: M.C. Plooij, Delft Robotics Institute, Faculty of Mechanical Engineering, Delft University of Technology, Mekelweg 2, 2628 CD Delft, The Netherlands Email: m.c.plooij@tudelft.nl

*Patent pending

the position of the joint directly determines the energy in the spring. This spring characteristic can be adjusted to match the task (see e.g. [8, 16, 18, 20]). The parallel spring then provides part of the torque required to perform the task, lowering the required actuator torques, and thereby reducing the energy consumption. Reduction of actuator torques should also allow for smaller gearbox ratios, leading to less gearbox friction, which again reduces the energy consumption.

Regular springs however, do not allow adjusting their characteristic during operation. This means that at any position, the amount of energy stored in the spring only depends on the design and not on the control. This greatly reduces the versatility of the robot in many ways, of which three are most prominent. First, when energy is stored in the spring, the spring exerts a torque on the joint, which is undesirable when the joint has to stand still. Secondly, the timing of energy capture and release cannot be controlled independently of the joint position. And thirdly, the energy that is stored in the spring while decelerating in one direction can only be used to accelerate in the opposite direction.

The solution to these problems is to make the energy inflow and outflow of the spring controllable. This could theoretically be realized by placing an infinitely variable transmission (IVT) between the joint and the spring, as proposed in [29]. However, there are no studies showing the working principle and effectiveness of such an IVT. Therefore, other researchers proposed to use locking mechanisms to control the energy inflow and outflow of the spring [11, 16, 17, 30–34]. Locking the spring when standing still prevents the spring from exerting torque on the joint, solving the first problem mentioned above [11, 16]. The second problem mentioned above is addressed by Haeufle et al. [17], who proposed a CPEA in which the parallel spring can be connected to a joint by a controllable clutch. They report a reduction of 80 % in the energy consumption of their emulated knee joint. However, the challenge that still has not been addressed is that the energy that is stored in the spring while decelerating in one direction can only be used to accelerate in the opposite direction. Solving this problem is crucial in order to be able to perform tasks like pick-and-place tasks. In such tasks, the task positions change constantly and could be on either side of the current position of the robot.

In order to solve this challenge, we recently proposed to use the Bi-directional Clutched Parallel Elastic Actuator [32] (BIC-PEA, see Fig. 1). The BIC-PEA consists of one differential mechanism, two locking mechanisms and one spring that is placed inside the differential mechanism. The parallel spring can be connected to the joint at an arbitrary position or speed when the kinetic energy has to be stored in the spring. This energy can be released at an arbitrary later point in time, accelerating the joint in any desired direction. This principle is suited for rest-to-rest motions, which we will study in this paper. At a recent conference, we presented the working principle of the BIC-PEA and showed the torque-displacement relationship of the prototype that we will also use in this paper [32].

In this paper, we extend our previous study in two ways. First, we analyze the capability of the BIC-PEA to reduce the energy consumption of robots by analyzing the energy consumption for a set of tasks. This analysis is supported by simulation and hardware experiments. Second, we provide a guideline for selecting the two most important parameters of the BIC-PEA: the spring stiffness and maximum spring displacement. Although the BIC-PEA provides more functionality than the CPEA, the goal is to reach a reduction similar to that reported for the CPEA [17].

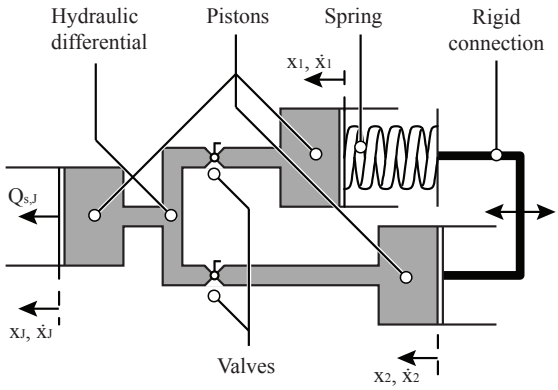

Figure 2. A schematic drawing of the concept of the BIC-PEA, visualized as a hydraulic system. It consists of a differential, a spring and two valves (locking mechanisms). The differential mechanism causes the joint piston to move with the sum of the velocities of the other two pistons. The valves can lock the two pistons. Note that for this hydraulic concept to work in practice, the pistons would have to be able to handle negative pressures, which would require more complicated, double-acting cylinders. However, in the geared concepts in this paper, this is not an issue.

The rest of the paper is structured as follows. Section II provides a more detailed explanation of the working principle of the BIC-PEA. Next, section III discusses the design of our prototype. Then, section IV explains our methods for analyzing the energy consumption in simulation and in hardware experiments. The results in sections V and VI show how implementation of the BIC-PEA can lead to a decrease in the energy consumption up to 65 %, depending on the specific task. The paper ends with a discussion in section VII and a conclusion in section VIII.

II. Working principle

In this section, we explain the working principle of the BIC-PEA in more detail. First, we will explain the components of the BIC-PEA (one differential mechanism, two locking mechanisms and a spring) and how they are connected. Second, we will explain the operating principle of the BIC-PEA. A schematic drawing of the BIC-PEA is shown in Fig. 2. This figure shows a hydraulic mechanism for explanation purposes. The final design of the BIC-PEA is a geared version and will be explained in section III-B.

A. Differential mechanism

A differential mechanism is a mechanism with three coupled axes. The coupling is described by one constraint that can be written in the form:

$$x_j = n_1 x_1 + n_2 x_2 \tag{1}$$

where n_1 and n_2 are constant positive transfer ratios, x_j is the position of the input and x_1 and x_2 are the positions of the

output of the differential. These three positions are the three axes of the differential mechanism. Examples of such mechanisms are a planetary gear, a planetary differential, a bevel-gear differential and a 'movable pulley and cables' differential. We call a differential mechanism ideal if $n_1 = n_2$, which is generally the case for the planetary differential, automotive differential and 'movable pulley and cables' differential. In the BIC-PEA, the input position x_j is connected to the joint of a robot, hence the subscript j.

B. Locking mechanisms

A locking mechanism is a component that can switch between allowing and preventing relative motion between two other components (see [33]). In the BIC-PEA, the two locking mechanisms are placed between the ground and the two output positions x_1 and x_2. The discrete states of the two locking mechanisms are denoted by L_1 and L_2, which have value 0 if the output position is locked to the ground and have value 1 if the output position is not locked. Using this notation, eq. (1) can be re-written in terms of velocities:

$$\dot{x}_j = n_1\dot{x}_1 + n_2\dot{x}_2 \tag{2}$$

with $\dot{x}_i = 0$ if $L_i = 0$, $i \in 1, 2$.

C. Spring

A spring is a compliant component with (in our case) two connection points. The potential energy that is stored in the spring is a function of the relative position of the two connection points. In the BIC-PEA, a spring is placed between the two output positions of the differential mechanism. Therefore, the displacement of the spring is equal to

$$\Delta x = x_1 - x_2 \tag{3}$$

where the positions are defined such that $\Delta x = 0$ is an equilibrium position of the spring. The potential energy in the spring is a function of this displacement:

$$E_s = f(\Delta x) \tag{4}$$

The generalized force $Q_{s,i}$ exerted by the spring on the i-th axis is given by

$$Q_{s,i} = -\frac{\partial \Delta x}{\partial x_i}\frac{\partial f(\Delta x)}{\partial \Delta x} \tag{5}$$

where force is defined in the same direction as position. Examples of commonly used springs are compression springs, extension springs, torsion springs and spiral springs. Most springs have a constant and positive stiffness, which means that $\dfrac{\partial f(\Delta x)}{\partial \Delta x}$ is a monotonically increasing and linear function of Δx:

$$\frac{\partial f(\Delta x)}{\partial \Delta x} = k\Delta x \tag{6}$$

where k is the spring stiffness. The apparent spring stiffness at the joint is k_j, which is equal to

$$k_j = \left(\frac{\partial \Delta x}{\partial x_j}\right)^2 k \tag{7}$$

and the maximum displacement of the spring is called Δx_{max}.

D. Operating principle

Using the two locking mechanisms, there are four modes of operation:

1. $\boldsymbol{L_1 = 1}$ **and** $\boldsymbol{L_2 = 1}$**:** The two output positions are free to move and therefore the spring deflection Δx is independent of the joint position x_j. Although the spring might deflect due to inertia and friction, these deflections are negligible as long as the spring stiffness is sufficiently large.
2. $\boldsymbol{L_1 = 0}$ **and** $\boldsymbol{L_2 = 1}$**:** Output position 1 is locked, meaning that $\dot{x}_1 = 0$. Since x_1 is now constant, the spring deflection linearly depends on the joint position. Combined with eq. (1), this results in:

$$\Delta x = c_1 - x_2 \tag{8}$$

$$= (1 + \frac{n_1}{n_2})c_1 - \frac{1}{n_2}x_j \tag{9}$$

where c_1 is equal to x_1 at the moment that x_1 was locked. Substituting in eq. (5) leads to:

$$Q_{s,j} = \frac{1}{n_2} \cdot \frac{\partial f(\Delta x)}{\partial \Delta x} \tag{10}$$

3. $\boldsymbol{L_1 = 1}$ **and** $\boldsymbol{L_2 = 0}$**:** Output position 2 is locked, meaning that $\dot{x}_2 = 0$. Since x_2 is now constant, the spring deflection again linearly depends on the joint position:

$$\Delta x = x_1 - c_2 \tag{11}$$

$$= \frac{1}{n_1}x_j - (1 + \frac{n_1}{n_2})c_2 \tag{12}$$

where c_2 is equal to x_2 at the moment that x_2 was locked. This leads to the generalized force:

$$Q_{s,j} = -\frac{1}{n_1}\frac{\partial f(\Delta x)}{\partial \Delta x} \tag{13}$$

4. $\boldsymbol{L_1 = 0}$ **and** $\boldsymbol{L_2 = 0}$**:** The two output positions are locked and thus the joint position is locked as well. If the spring is deflected, it will remain deflected while being in this mode of operation.

From eqs. (10) and (13), it follows that for the same deflection of the spring, the joint force can be negative or positive. Now suppose that $\dot{x}_j$ is positive. If we want to decelerate the joint, we switch to mode 3, where the force on the joint is negative. Once the joint is decelerated to zero velocity and the kinetic energy is transferred to potential energy in the spring, we switch to mode 4. From mode 4, we can release the potential energy by accelerating in positive or negative direction (respectively mode 3 and 2). Similarly, if $\dot{x}_j$ had been negative, we would have switched to mode 2 to decelerate the joint.

From eqs. (10) and (13), it is also clear why an ideal differential is advantageous: if $n_1 = n_2$, the stiffnesses while accelerating in positive and negative direction are identical.

III. Prototype Design

We built a prototype of the BIC-PEA in order to test how much it can reduce the energy consumption of a standard robotic joint actuated by a DC motor. In this section we first

discuss selection of the spring. Then, we describe the hardware design of the BIC-PEA. And finally, we present a model and show how the model corresponds to previous measurements in [32].

A. Spring selection

The spring is one of the most important component of the BIC-PEA. Selection of the spring will influence the amount of energy that is saved in certain tasks. The tasks are defined by a certain allocated motion duration t_f and distance to move x_f. We hypothesize that the savings will be highest in tasks where the 'natural motion duration' t_n corresponds with the required motion duration t_f. The natural motion duration is the time it takes to move from the start to the goal position in a frictionless system, without actuation. We will verify the hypothesis in simulation in section V-C. Following this hypothesis, we will now calculate the natural motion duration for a frictionless system with BIC-PEA and without actuation and derive the spring stiffness that leads to equality of t_f and t_n.

Therefore, let's assume a frictionless system in which the only force that acts is the spring force and where the spring is exploited up to a maximum excursion, measured at the joint axis $\Delta x_{j,max}$. Furthermore, assume an initial and final velocity of zero and infinitely fast switching locking mechanisms. The motion of this system can be split into three phases: an acceleration phase, a phase with constant velocity and a deceleration phase. The first and last phase together form half of an oscillation of a linear spring-mass system, meaning that the combined duration of those two phases is equal to

$$t_1 + t_3 = \pi \sqrt{\frac{J}{k_j}} \tag{14}$$

where J is the inertia of the robot. The velocity during the second phase is

$$\dot{x}_j = \Delta x_{j,max} \sqrt{\frac{k_j}{J}} \tag{15}$$

and since the distance that has to be traveled in the second phase is $x_f - 2\Delta x_{j,max}$, this phase has a duration of

$$t_2 = \frac{x_f - 2\Delta x_{j,max}}{\Delta x_{j,max} \sqrt{\frac{k_j}{J}}} \tag{16}$$

The total time it takes for this system to move to x_f is

$$t_n = t_1 + t_2 + t_3 = \sqrt{\frac{J}{k_j}} \left(\pi - 2 + \frac{x_f}{\Delta x_{j,max}} \right) \tag{17}$$

This t_n is the natural motion duration. Now assuming that this time corresponds with the motion duration (i.e. $t_n = t_f$), we can write the stiffness as function of the system and task parameters t_f and x_f:

$$k_j = J \left(\frac{\frac{x_f}{\Delta x_{j,max}} + \pi - 2}{t_f} \right)^2 \tag{18}$$

When choosing the BIC-PEA parameters $\Delta x_{j,max}$ and k_j, two things should be taken into account. First, the minimum distance $x_{f,min}$ that the BIC-PEA should move is twice the maximum displacement of the spring $\Delta x_{j,max}$. Therefore, this maximum spring displacement should be chosen to match the smallest distance that the system is expected to move:

$$\Delta x_{j,max} = \frac{1}{2} x_{f,min} \tag{19}$$

Shorter springs are undesirable because they are expected to lead to greater losses due to backlash.

Second, since the energy savings are expected to drop for tasks that are slower or faster than the natural motion duration, k_j should be optimized to fit the different task parameters. A good approximation is to take the average optimal k_j. This means, finding the mean k_j for all expected tasks combinations of $x_{f,i}$ and $t_{f,i}$ using

$$k_j = \frac{1}{N} \sum_{i=1}^{N} J \left(\frac{\frac{2x_{f,i}}{x_{f,min}} + \pi - 2}{t_{f,i}} \right)^2 \tag{20}$$

where N is the number of expected task combinations. Similarly to short springs, stiff springs are unwanted because they incur extra losses due to backlash and plastic collisions.

B. Mechanical design

In this section, we explain the design of our hardware prototype (see Fig. 1). A schematic drawing of the design is shown in Fig. 3. We respectively discuss the differential mechanism, the spring, the locking mechanisms and the mechanical properties.

As a differential mechanism, we use a planetary differential (see Fig. 3). The positions and velocities in this mechanism are rotational. Therefore, the generalized forces are actually torques. A planetary differential consists of two internal gears, one or multiple pairs of planet gears and a joint axis. Within one pair of planet gears, each gear engages with a different internal gear and the gears engage with each other. Our prototype has two pairs of planet gears, as can be seen in Fig. 4b. The angular displacements x_1 and x_2 of the separate sides of this planetary differential are described by:

$$x_1 = x_j + r_p x_{p1} \tag{21}$$

$$x_2 = x_j + r_p x_{p2} \tag{22}$$

where r_p is the effective radius of the planet gears and x_{p1} and x_{p2} are the positions of the planet gears (see Fig. 3). Since the two planets mesh with each other such that $x_{p1} = -x_{p2}$, the overall motion is described by:

$$x_j = \frac{1}{2} x_1 + \frac{1}{2} x_2 \tag{23}$$

This differential mechanism is an ideal differential since $n_1 = n_2 = 0.5$.

We chose to use a torsion spring with a spring stiffness of 0.17 Nm/rad and a maximum displacement of 0.5π rad. We attached two pegs to each side of the spring to connect to the internal gear (see Fig. 4a). The parameters of the BIC-PEA were chosen for the task with a distance to move of x_f = 2π rad and a motion duration of t_f = 1 s.

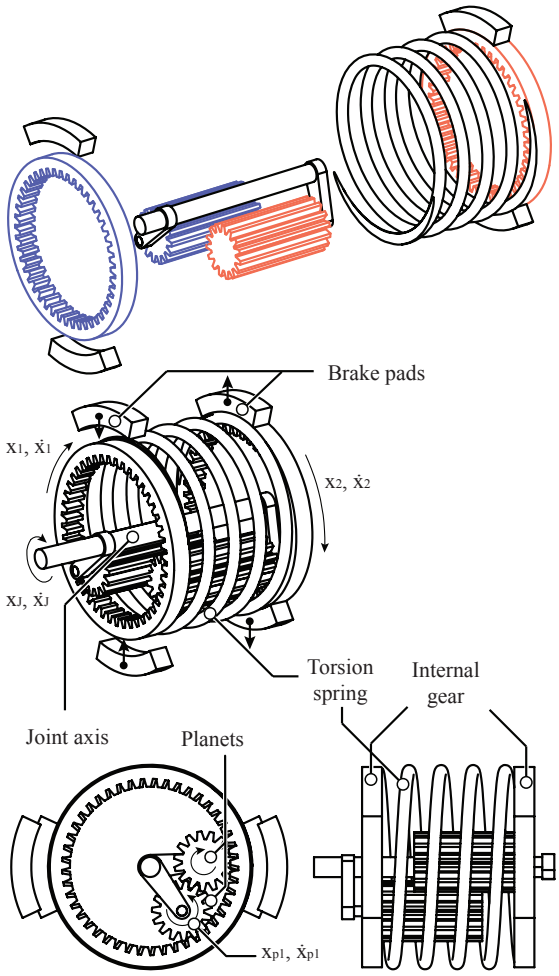

Figure 3. A schematic drawing of the final design of the BIC-PEA. It consists of a planetary differential, a torsion spring and two brakes. The planetary differential consists of two internal gears, two planet gears and one planet carrier (the joint axis). The planets have a lateral offset, such that each planet meshes with the different internal gear of the corresponding color and they mesh with each other in between the internal gears. The planet axes are connected to the joint axis by cranks so that the distances between the joint axis and the planet axes are fixed. The planets can rotate around their axes independent from the rotation of the joint axis. The spring connects the two internal gears. The differential mechanism causes the joint axis to rotate with the average velocity of the two internal gears. The brakes can lock the internal gears with respect to the ground.

In order to test the spring mechanism, we used two large brakes as locking mechanisms to lock the internal gears. These brakes consist of rubber plates that are each pushed against a Vulka SF-001 braking disk by a solenoid (see Fig. 5).

The BIC-PEA without brakes as shown in Fig. 1 weighs 202 g and fits in a cylinder with a length of 51 mm and a diameter of 45 mm. The transfer ratio of the joint axis to the spring (when one brake is locked) is 1:2. This means that the apparent spring stiffness at the robot joint is 0.68 Nm/rad. It has a peak torque of approximately 1.5 Nm and can store 0.77 J.

C. Modeling the BIC-PEA

In [32], the torque-displacement relationship and the friction of the BIC-PEA are measured. In order to generate energy-optimal trajectories, a model is required. We model the BIC-PEA in mode 2 and 3 as

$$Q_{s,j} = k_j(x_0 - x_j) - T_c \text{sign}(\dot{x}_j) \tag{24}$$

where x_0 is the joint's position when the spring is in equilibrium and T_c is the Coulomb friction torque. Coulomb friction is mainly generated by the gears and is the main cause for hysteresis in the mechanism. We used the Nelder-Mead simplex direct search algorithm of `fminsearch` in MATLAB to identify the values for k_j and T_c that lead to the least squared error between measurements [32] and model. The obtained values are k_j = 0.71 Nm/rad and T_c = 0.12 Nm. The fit has a root mean squared error of 0.08 Nm and a peak error of 0.17 Nm. In mode 1, $Q_{s,j}$ is equal to zero and in mode 4, the acceleration of the joint is zero.

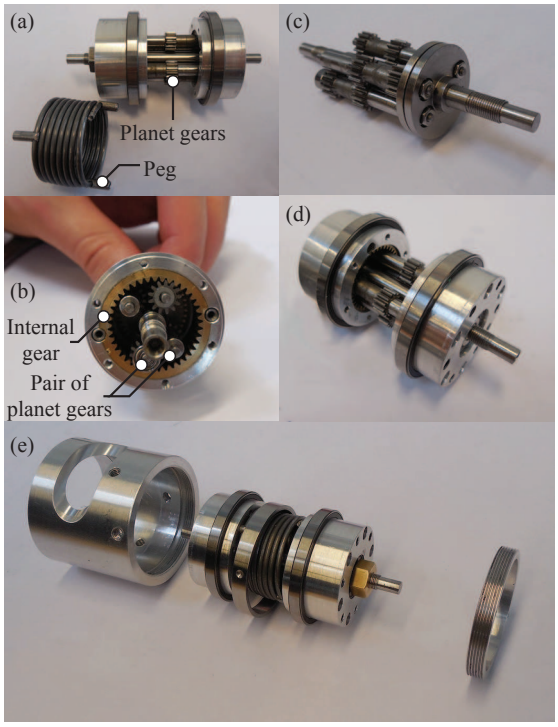

Figure 4. Photographs of the inside of the prototype. Note that the focal length makes the prototype appear larger than it is.

IV. Experimental Setup

In this section we explain the experimental setup we used to measure the reduction in energy consumption. First, we describe the measurement setup. Then, we explain how we find energy-optimal trajectories in simulation. And finally, we describe the hardware experiments.

A. Measurement setup

Fig. 5 shows the test setup we used to analyze the energy consumption. It consists of a Maxon RE-30 brushed DC motor that connects to a body with inertia through a timing belt. The inertia is represented by an aluminum tube of length 650 mm that connects to the joint in its center. At both end points of the tube, a brass block is placed inside the tube to increase the

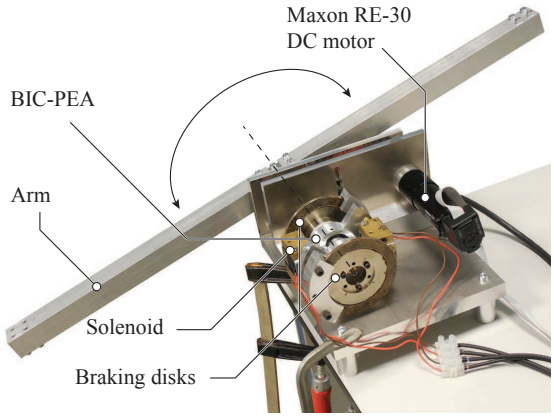

Figure 5. The setup to test the influence of the BIC-PEA on the energy consumption. It consists of a symmetric arm that rotates in a vertical plane. When the BIC-PEA is attached, it directly connects to the axle of the arm. A Maxon RE30 DC motor with a gearbox of 1:18 drives the system through a timing belt.

Table I
THE MODEL PARAMETERS OF THE ONE DEGREE OF FREEDOM TEST SETUP. THE VALUES ARE OBTAINED THROUGH A SYSTEM IDENTIFICATION OF THE SETUP.

Parameter arm	Symbol	Value
Inertia	J	0.029 kgm^2
Coulomb friction	T_{cf}	0.06 Nm
Torque-dependent friction	μ_{tf}	21 %
Torque constant	k_t	25.9 mNm/A
Motor resistance	R	1.5 Ω
Gearbox ratio	n	1:18
Spring stiffness	k_j	0.71 Nm/rad

inertia. This setup is not influenced by gravity. We chose such a setup because it was already shown in [13] that gravity can be compensated by parallel springs. The motor was chosen based on availability. The identified parameters of the test setup are listed in Table I. We used a gearbox ratio of 1:18 because initial simulations showed that this ratio leads to the lowest energy consumption when the BIC-PEA is not attached. Gearbox selection is discussed further in section VII-D.

B. Simulation experiments

Since we are focusing on rest-to-rest motions, the task that has to be performed is to move from one position to another, both with zero velocity. First, we analyzed how the performance depends on the two task parameters t_f and x_f. Therefore, we varied t_f between 0.7 s and 1.7 s and x_f between π rad and 3π rad.

Secondly, we varied the stiffness, to verify the stiffness selection hypothesis in section III-A. Meanwhile, we keep Δx_{max} constant. While varying the stiffness, we obtain the tasks for which the energy savings are maximal. If the hypothesis is true, these tasks satisfy eq. (17).

In order to fairly compare the system with and without the BIC-PEA, we have to know how it should move in order to consume as little energy as possible in each case. Therefore, we used optimal control to find energy-optimal trajectories off-line. The model of the arm that we used is:

$$\ddot{x}_j = \frac{T_m + Q_{s,j} + T_f}{J} \tag{25}$$

where T_m is the torque applied by the motor, T_f is the friction torque and J is the total inertia about the joint. The motor torque is equal to

$$T_m(t) = k_t n I(t) \tag{26}$$

where I is the current through the motor, k_t is the torque constant of the motor and n is the transfer ratio of the gearbox. T_f is equal to

$$T_f = -(T_{cf} + \mu_{tf}|T_m|)\text{sign}(\dot{x}_j) \tag{27}$$

where T_{cf} and μ_{tf} are the Coulomb friction torque and the torque-dependent friction coefficient respectively.

We used the optimal control software package GPOPS-II [35] to find energy-optimal trajectories between the two positions. As solver we used the SNOPT version that comes with GPOPS II. The cost function that we used is the integral over the electrical motor power P, which is equal to

$$P = T_m \dot{x}_j + I^2 R \tag{28}$$

where R is the terminal resistance of the motor windings. Note that the power can become negative when the motor torque opposes the velocity. This would lead to a decrease in the cost function and models recapturing energy electrically. Therefore, using this cost function, we compare the energy consumed by the system with the BIC-PEA to a system that can use the motor as a generator. The optimization has a free end time t^* with a maximum of t_f. The overall optimal control problem is described by:

$$\begin{aligned} \underset{T_m(t)}{\text{minimize}} \quad & \int_0^{t^*} P \mathrm{d}t \\ \text{subject to} \quad & t^* \leq t_f \\ & x(0) = 0 \\ & x(t^*) = x_f \\ & \dot{x}(0) = \dot{x}(t^*) = 0 \end{aligned} \tag{29}$$

Note that the measure for the energy consumption does not include the energy consumed by the locking mechanisms. This choice will be discussed in section VII-C.

We assume that it is optimal to switch the BIC-PEA depending on the initial and the final positions. Therefore, for $x_j < \Delta x_{max}$ the generalized force $Q_{s,j}$ is equal to

$$Q_{s,j} = k_j(\Delta x - x_j) - T_c \text{sign}(\dot{x}_j) \tag{30}$$

for $x_j > x_f - \Delta x_{max}$, it is equal to

$$Q_{s,j} = k_j(x_f - \Delta x - x_j) - T_c \text{sign}(\dot{x}_j) \tag{31}$$

and $Q_{s,j}$ = 0 otherwise.

C. Hardware experiments

In the hardware experiments, the energy-optimal trajectories that were calculated off-line, are followed by a manually tuned PD controller in combination with the feedforward controller that follows from the optimization. For the system without the BIC-PEA attached, the tuned controller gains are $[K_P, K_D]$ = [1, 0.2][Nm/rad, Nms/rad]. In the system with the BIC-PEA, a smaller proportional gain appeared to be optimal: $[K_P, K_D]$ = [0.5, 0.2][Nm/rad, Nms/rad].

The solenoid brakes have a switching time that is not negligible. Therefore, they are switched at a fixed duration before reaching the switching positions. When disengaging, the brake is switched 0.1 s before reaching the switching position. When engaging, this is 0.02 s.

The trajectories that will be tested on the hardware setup have a motion duration that varies between 0.7 s and 1.7 s and a fixed distance to move of 2π rad. In practice, a task description will consist of several times to move and moving distances. To show the versatility of the BIC-PEA, we composed a task where the arm has to move between four positions. First, it moves from 0 rad to 3π rad in 1 s. Then, it moves to 4.5π rad in 1.5 s. Next, it moves to 1.5π rad in 1.5 s. And finally, it moves back to 0 rad in 1 s.

The energy consumption of those motions is calculated by numerically integrating the electrical power:

$$E = \int_0^{t_f} UI \mathrm{d}t \tag{32}$$

where U is the voltage that is applied on the motor. Note that this energy consumption does not include the energy consumed by the brakes. There are two types of motions, which we will call *type 1* and *type 2*. In motions of type 1, the next motion continues in the same direction as the previous motion. So after deceleration, the arm will accelerate while moving in the same direction. In motions of type 2, the next motion is in the opposite direction of the previous motion. This type of motion leads to back-and-forth motions. We repeated every task 18 times: 9 times for type 1 and 9 times for type 2. The results are then averaged.

V. Simulation results

In this section, we first show the results of the optimal control study for a nominal task. Then, we show the results for multiple task parameters. And finally, we verify the stiffness selection hypothesis from section III-A.

A. Energy savings for a nominal task

Fig. 6 shows the optimized motions for moving one revolution in one second, with and without the BIC-PEA attached. As can be seen in Fig. 6d, when the BIC-PEA is attached, the robot consumes 72 % less energy. Fig. 6c shows that the robot with BIC-PEA is decelerating while the motor does not apply a negative torque. This deceleration is mainly caused by the negative torque of the spring at this point.

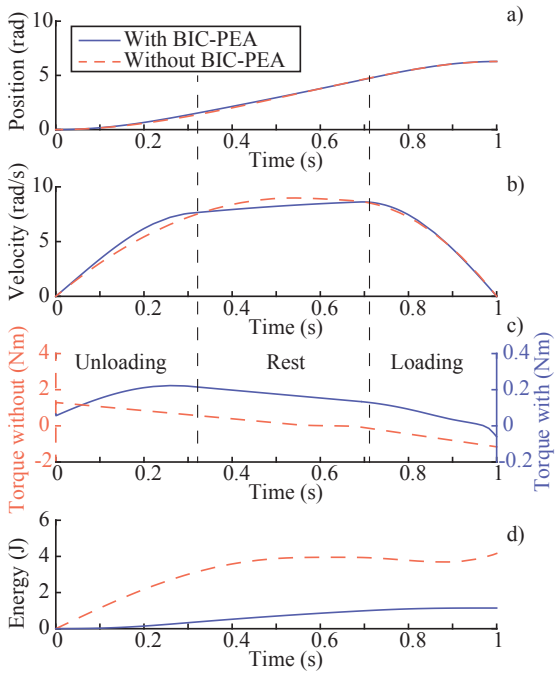

Figure 6. The optimized trajectories to move one rotation in one second with and without the BIC-PEA attached. Note that in c), the torques for the motion with BIC-PEA are multiplied by a factor 10. The vertical striped lines indicate the switching times of the locking mechanisms. Therefore, they divide the motion into three phases: a phase in which the spring unloads, a phase in which the spring is in rest and a phase in which the spring is loading. Please note the difference in scale in c.

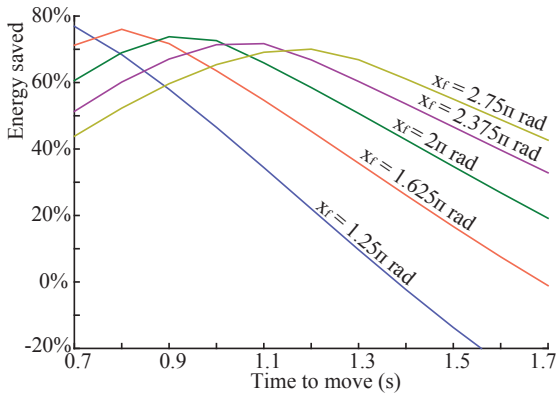

Figure 7. The energy savings in simulation as function of the task parameters. For every distance to move, there is a motion duration that leads to approximately 73 % energy savings. This maximum percentage of energy saved decreases when the distance to move increases.

B. Influence of task parameters

Fig. 7 shows the energy savings as function of the task parameters. This figure shows that the maximum percentage of energy that can be saved is approximately 73 % and that there is a manifold of tasks in which this can be achieved. The figure shows that the savings for other tasks are lower, but for a considerable amount of tasks, the system with BIC-PEA still consumes less energy than the system without BIC-PEA.

C. Influence of the spring stiffness

Fig. 8 shows two sets of data. First, it shows the manifolds for x_f and t_f that follow from eq. (18) for nine different

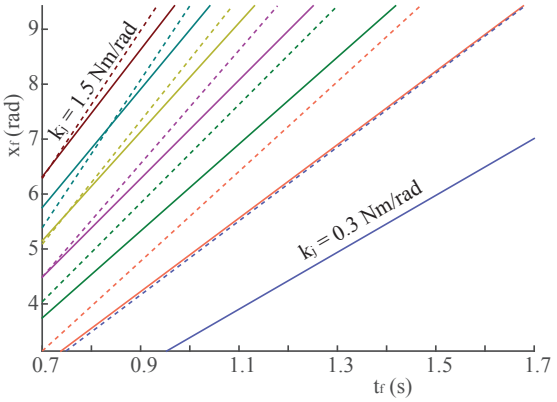

Figure 8. The optimal task manifold for nine different stiffnesses in simulation. The figure shows the manifold both from an idealized model (solid lines) and from simulations with a realistic model (dashed lines). It shows that the two models are comparable, especially at high stiffnesses.

stiffnesses. These manifolds represent the natural motion of the system. Second, it shows the manifolds with the maximum energy savings in simulation for the same nine stiffnesses. It shows that the two manifolds are similar, especially at high stiffnesses. The similarity between the analytical manifolds and the optimal manifolds in simulation shows that the tasks in the optimal manifolds in simulation indeed coincide with the natural motion of the system. The differences between the two sets of manifolds is due to the effects of friction, which is larger at low stiffnesses.

VI. Hardware results

Fig. 9a shows the energy that is consumed by the hardware setup with and without the BIC-PEA attached. The figure shows that the results in simulation and hardware experiments are comparable. For the system without the BIC-PEA attached, the energy consumption decreases when the motion duration is increased. For the system with BIC-PEA, the same holds until a motion duration of approximately 1 s, after which the consumed energy is constant. The latter is caused by the fact that for larger times to move, the energy-optimal trajectory is to move in approximately 1 s and then stand still at the goal position.

Fig. 9b shows the percentage of energy that is saved by implementing the BIC-PEA as function of the motion duration. The figure shows the same trend in simulation and hardware experiments: there is a peak at a time to move of approximately 0.9 s and the savings decrease when the time to move is increased. The peak in hardware experiments in lower than in simulation: 65 % in hardware experiments and 73 % in simulation.

Fig. 10 shows the hardware results for performing the realistic task. Figs. 10a and 10b show the positions as function of time for the system with and without the BIC-PEA for 10 runs. Fig. 10c shows the energy consumed over time. The system without BIC-PEA consumed 25.0 ($\pm$ 0.1) J to complete the task. The system with BIC-PEA consumed 11.8 ($\pm$ 1.4) J. This means that implementation of the BIC-PEA resulted in a 53 % lower energy consumption for this task.

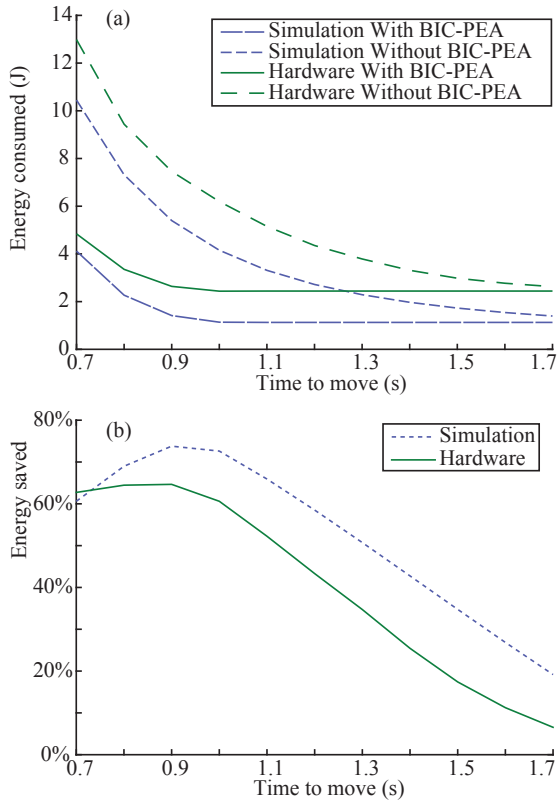

Figure 9. The hardware results, including a comparison to the simulation results. a) The energy consumption of the arm as function of the motion duration for a distance to move of 2π rad. The lines show the energy consumed in simulation and in hardware experiments for the system with and without the BIC-PEA attached. b) The energy savings of the arm as function of the time to move for a distance to move of 2π rad. The lines show the energy saved in simulation and in hardware experiments.

VII. Discussion

In this paper, we presented the concept of the BIC-PEA and showed its potential in reducing the energy consumption of robots. In this section we discuss the performance, the applicability, the use of locking mechanisms, selection of the gearbox and other embodiments of the BIC-PEA.

A. Performance

The simulation results showed that theoretically 73 % energy can be saved by implementing the BIC-PEA. Hardware results showed the same trends as simulation results, but the energy savings were maximally 65 % and 53 % for a realistic task. Furthermore, in hardware experiments, the robot consumed more energy than in simulation. In the system without the BIC-PEA, this is caused by an imperfect model, introducing the need for feedback. In the system with BIC-PEA, another cause for the larger energy consumption is the imperfectness of the locking mechanisms. Since the brakes have a non-zero switching time and sometimes slip slightly, the efficiency of the BIC-PEA decreases.

In hardware experiments, the energy consumption was measured for rest-to-rest motions of *type 1* and *type 2*. In the results, the energy consumptions of these two types of motions were averaged. It should be noted that the results

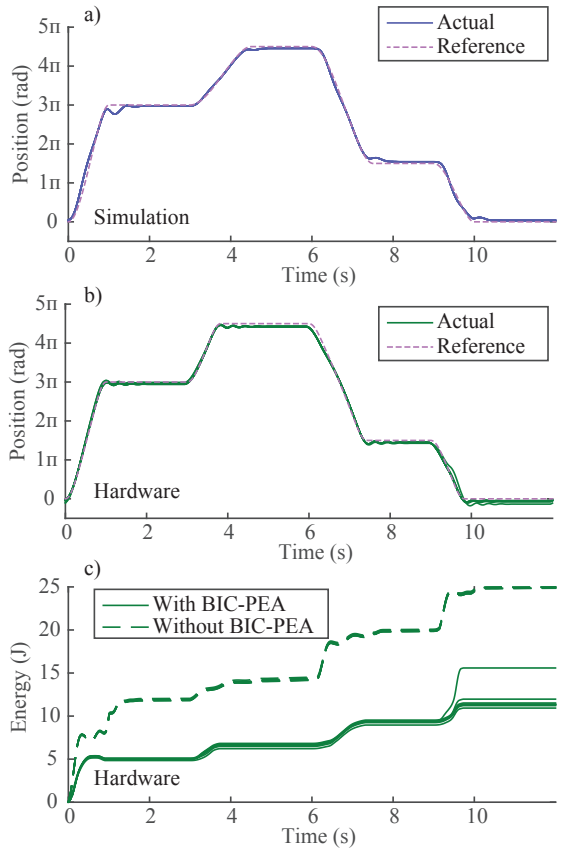

Figure 10. The hardware results for performing a realistic task. The arm moves from 0 rad to 3π rad to 4.5π rad to 1.5π rad and then back to 0 rad. The times to move are 1 s, 1.5 s, 1.5 s and 1 s. a) The position of the arm without the BIC-PEA. b) The position of the arm with the BIC-PEA. c) The energy consumed over time for the system with and without the BIC-PEA.

were quantitatively different. For instance, for the motion with a motion duration of 0.9 s, the energy consumptions for the system with BIC-PEA attached were 2.94 ($\pm$0.20) J and 2.34 ($\pm$0.46) J for type 1 and type 2 motions respectively. For the system without BIC-PEA attached this was 8.20 ($\pm$0.57) J and 6.71 ($\pm$0.13) J. Although the exact energy consumptions were different, the energy savings for both types of motions are similar: 64 % and 65 % respectively.

The fact that the energy consumption of the two types of motions is different is caused by steady-state errors at the goal positions. As is also visible in Fig. 10, the position has a steady-state error by stopping just before reaching the goal position. When the next motion is in the opposite direction, the arm starts with a lead with respect to the reference. When the next motion is in the same direction, the arm starts with a lag. The feedback control effort it takes to compensate for this lag causes the higher energy consumption in continuing motions.

The two main losses in robotic arms are friction and copper losses. The energy consumption of the arm without BIC-PEA consists for 71 % of copper losses and 29 % of friction losses, for the motion displayed in Fig. 6. When attaching the BIC-PEA, the friction losses remain approximately equal, while the copper losses are decreased. The copper losses then account for 11 % of the energy consumption and the friction accounts for 89 %. Therefore, future research should focus on reducing the friction losses in robots in order to further reduce the energy consumption.

As mentioned in the introduction, there are two concepts that compete with the BIC-PEA in terms of energy efficiency. First, mechanical energy could be recaptured electrically, such as in the Cheetah robot [9]. The advantage of this is that the energy flow remains fully controllable. However, as mentioned in the introduction, the energy that can be saved using this approach is only 40 %. Furthermore, the 65 % savings achieved with the BIC-PEA are in comparison with a system that also recaptures energy electrically (note the descent of the energy consumed at the end of the motion in Fig. 6d). To achieve the 40 % reduction, specialized motors are required. On the other hand, it should be noted that the energy savings of the BIC-PEA come at the price of increased mass and size of the robot. The added mass of our prototype is 202 g (plus the mass of the locking mechanisms, see below) and the added size is 81 cm^3 (plus the size of the locking mechanisms, see below). As a reference, this is equal to the volume and mass of the motor that is used in the test set-up. For a fixed-base system like an industrial robot, the added mass on the root joint is irrelevant. For the other joints and for mobile systems, the drawbacks of the an increase in mass have to be weighed carefully against the achievable energy savings. For example, while wheeled platforms would likely benefit, for systems that perform flight phases, like the Cheetah, the concept might be less attractive.

A second concept that competes with the BIC-PEA in terms of energy efficiency is the existing clutched parallel elastic actuator (CPEA) [17]. This CPEA has shown to be able to decrease the energy consumption with 80 %. However, such a CPEA cannot use the potential energy in the spring to accelerate in any desired direction and therefore decreases the versatility of the arm. For instance, the task in Fig. 10 cannot be performed using this existing CPEA.

So far, we did not consider how implementation of the BIC-PEA influences the precision of the robot. The importance of precision depends on the specific task, and within tasks often on the workspace location. While industrial robots often move very fast to a particular location, the precision is most relevant when they perform manipulation at that location, so within a small region of the workspace. Many tasks can be performed with the precision of our system with the BIC-PEA. Furthermore, there is no fundamental reason why the precision should decrease with a BIC-PEA. It is true that our specific implementation (with slow responding brakes) decreases the precision. But even in tasks when precision is required occasionally, the robot could choose to only lock the second locking mechanism when a certain precision is reached. Note that this most probably would increase the energy consumption for that stroke.

B. Applicability

The BIC-PEA is suitable for all robots that perform rest-to-rest motions. The most common example of such a task in

industry is a pick-and-place task with a robotic arm. However, the applications of BIC-PEAs far exceed robotic arms. In fact, all machines that decelerate and accelerate again in a repetitive manner would benefit from an efficient way of energy recapture. For instance, one could imagine that a wheeled robot that constantly has to come to a standstill and then accelerate again could benefit from implementation of a BIC-PEA. Also, a manufacturing process where belts transport a batch of products in intermittent fashion (to allow discrete operations to be performed on the products) could benefit.

Clutched elastic actuators are not applicable in all types of robots. For instance, due to the switching, a user needs to expect a negative effect on bandwidth or transparency of the device, which is relevant for applications in for instance haptics.

Future research on CPEAs could focus on other configurations with more locking mechanisms that increase the applicability of the BIC-PEA. For instance, an extra clutch between the axis of the robot and the input shaft of the BIC-PEA would allow for the robot to move while the spring remains loaded. This could also be used to increase the precision of the robot, because after the spring has come to a stand-still, the robot joint can still be moved. Another option to increase the position control is to use multi-stage actuation. A second direction for future research is the use of various types of elastic elements. One of the fundamental limitations of springs is the energy that can be stored, which depends on the material and qualitative geometry. An interesting option would be to investigate axially loaded rubber bands [8]. Finally, control design for hybrid systems with both continuous and discrete states is still an open field of research.

C. Locking mechanisms

In the current prototype, we used solenoid actuated brakes to lock the internal axes of the differential mechanism. In the results, we excluded the energy consumption, mass and size of the solenoids, which assumes an ideal locking mechanism. In practice however, the solenoids consume 3.6 W per solenoid when active. Depending on the specific task, the energy consumption of the current brakes is lower or higher than the amount of energy saved. But in general, the energy consumption of the brakes was detrimental to the performance of the BIC-PEA. Furthermore, the brakes add mass and volume to the prototype: approximately 400 g and 140 cm^3 in total. The reason for excluding the energy consumption, mass and volume from the main results is that simultaneously with the BIC-PEA, we developed a new type of clutch called statically balanced brakes [36]. Such clutches require 96 % less actuation force than regular brakes, reducing the energy consumption of the brakes significantly. Two copies of the currently best statically balanced brake would weigh 184 g and have a volume of 225 cm^3. Another type of clutch that is being developed at the moment is the electroadhesive clutch. The prototope of Diller et al. [37] consumes 0.6 mW during a similar task and has a peak torque of 7.3 Nm, which is more than the peak torque of the BIC-PEA. Since this energy consumption is negligible, we expect that with these new types of brakes, the reduction in energy consumption will be close to the 65 % reported in this paper.

Next to statically balanced brakes, also various other types of locking mechanisms have been used in robotics [33]. An interesting direction of future research would be to consider different locking mechanisms. For instance in some applications, active latches can be used in which the position of locking and unlocking can be set by an actuator. This research might also focus on the accuracy of the timing of the locking mechanisms, since that proved to be important in the hardware experiments.

D. Gearbox selection

In this paper, we used the same gearbox ratio for the system with and without the BIC-PEA. In the introduction we stated that reduction of actuator torques should also allow for smaller gearbox ratios, leading to less gearbox friction, which further reduces the energy consumption. We conducted an optimization to confirm this. This optimization is the same as the one used for Fig. 7, but with a varying gearbox ratio instead of a varying task description. The result confirmed our expectation: showing a minimum energy consumption in the neighborhood of 1:6.2 for the task of moving 2π rad in 1 s with the BIC-PEA attached. However, there are always inaccuracies in the simulation model, resulting in the need for feedback. With such a small gearbox ratio, the feedback control action leads to high copper losses. Initial hardware results showed that these copper losses were so high that the system with BIC-PEA had a higher energy consumption than the system without the BIC-PEA. Since without the BIC-PEA, the optimization showed that a gearbox ratio of 1:18 would be optimal, we decided to also use this gearbox ratio for the system with BIC-PEA.

E. Other configurations

There are numerous configurations of BIC-PEAs that all have the same functionality. However, there are two configurations that we would like to mention because of their distinct advantages: the hydraulic and the planetary gear versions.

A schematic drawing of a hydraulic version is shown in Fig. 2. The advantage of this configuration is that both the differential and the locking mechanisms are relatively simple: the differential is a three-way tube and the locking mechanisms are valves. Of course, such a system would only work if the leakage and friction are minimal.

The planetary gear version is shown in Fig. 11. The advantage of this configuration is that the differential is relatively compact. The disadvantage however is that a planetary gear is not an ideal differential as described in section II.

A third configuration that could be interesting is the concept with a bevel-gear differential. We rejected this concept because of two reasons. First, the spring would have to be placed in between the two bevel gears on the side. An initial design study showed that this would make the concept relatively large. Second, the bevel-gear differential is T-shaped, while most actuators are built in a cylindrical shape. In order to stay close to current actuators, we chose a concept that has a cylindrical shape.

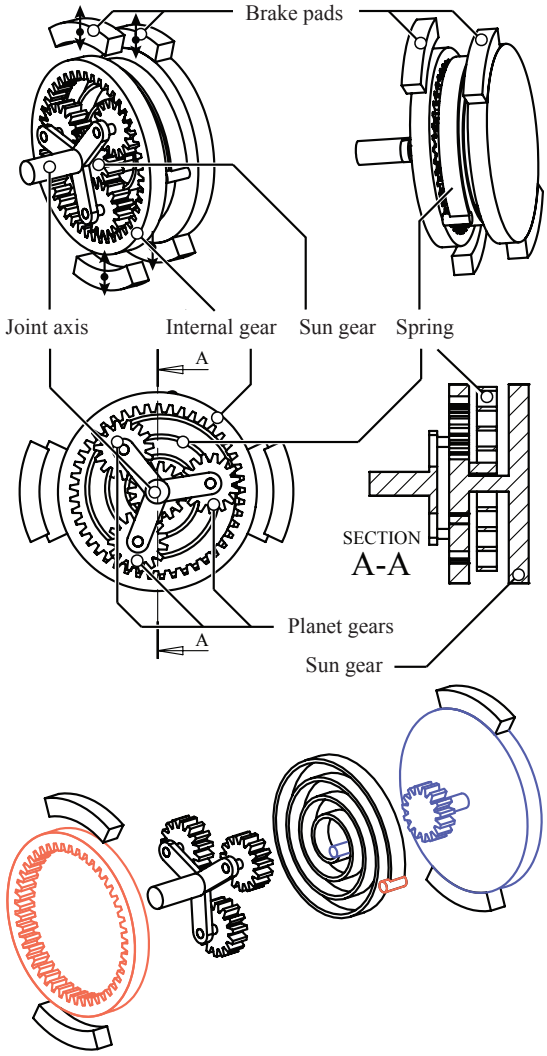

Figure 11. A planetary gear version of the BIC-PEA, which is compact in axial direction. The spring is placed between the sun and the internal gear of the planetary gear, as indicated by the corresponding colors.

VIII. Conclusion

In this paper, we presented the concept of the Bi-directional Clutched Parallel Elastic Actuator (BIC-PEA). The BIC-PEA is suitable for implementation in robots that perform rest-to-rest motions such as pick-and-place robots. We conclude that using the BIC-PEA, the energy consumption of such robots can be reduced significantly without compromising their capabilities. Results show that implementing the BIC-PEA leads to a decrease of the energy consumption up to 73 % in simulation, in comparison to the same system that also allows for recapturing energy electrically. In hardware experiments a reduction of 65 % was reached. This is larger than all other concepts with the same functionality.

Acknowledgement

This work is funded by research programme STW, which is (partly) financed by the Netherlands Organisation for Scientific Research (NWO), and by a Marie-Curie career integration grant PCIG13-GA-2013-618899.

References

[1] D. Meike and L. Ribickis, "Energy efficient use of robotics in the automobile industry," in *Advanced Robotics (ICAR), 2011 15th International Conference on*, June 2011, pp. 507–511.

[2] Y. Mei, Y.-H. Lu, Y. Hu, and C. S. G. Lee, "Energy-efficient motion planning for mobile robots," in *Robotics and Automation, 2004. Proceedings. ICRA '04. 2004 IEEE International Conference on*, vol. 5, 2004, pp. 4344–4349 Vol.5.

[3] S. Collins, A. Ruina, R. Tedrake, and M. Wisse, "Efficient bipedal robots based on passive-dynamic walkers," *Science*, vol. 307, no. 5712, pp. 1082–1085, 2005.

[4] J. E. Pratt, B. T. Krupp, C. J. Morse, and S. H. Collins, "The roboknee: an exoskeleton for enhancing strength and endurance during walking," in *Robotics and Automation, 2004. Proceedings. ICRA'04. 2004 IEEE International Conference on*, vol. 3. IEEE, 2004, pp. 2430–2435.

[5] A. M. Dollar and H. Herr, "Lower extremity exoskeletons and active orthoses: challenges and state-of-the-art," *Robotics, IEEE Transactions on*, vol. 24, no. 1, pp. 144–158, 2008.

[6] S. Au and H. Herr, "Powered ankle-foot prosthesis," *Robotics & Automation Magazine, IEEE*, vol. 15, no. 3, pp. 52–59, 2008.

[7] F. Sup, A. Bohara, and M. Goldfarb, "Design and control of a powered transfemoral prosthesis," *The International journal of robotics research*, vol. 27, no. 2, pp. 263–273, 2008.

[8] S. Pfeifer, A. Pagel, R. Riener, and H. Vallery, "Actuator with angle-dependent elasticity for biomimetic transfemoral prostheses," *Mechatronics, IEEE/ASME Transactions on*, vol. PP, no. 99, pp. 1–11, 2014.

[9] S. Seok, A. Wang, M. Y. Chuah, D. Otten, J. Lang, and S. Kim, "Design principles for highly efficient quadrupeds and implementation on the mit cheetah robot," in *Robotics and Automation (ICRA), 2013 IEEE International Conference on*, May 2013, pp. 3307–3312.

[10] J. Herder, "Energy-free systems: Theory, conception and design of statically balanced spring mechanisms," 2001.

[11] V. I. Babitsky and A. Shipilov, *Resonant robotic systems*. Springer, 2003.

[12] S. Shirata, A. Konno, and M. Uchiyama, "Design and evaluation of a gravity compensation mechanism for a humanoid robot," in *Intelligent Robots and Systems (IROS), IEEE/RSJ International Conference on*, Oct 2007, pp. 3635–3640.

[13] M. Vermeulen and M. Wisse, "Intrinsically safe robot arm: Adjustable static balancing andlow power actuation," *International Journal of Social Robotics*, vol. 2, no. 3, pp. 275–288, 2010.

[14] J. D. Karssen and M. Wisse, "Running with improved disturbance rejection by using non-linear leg springs," *The International Journal of Robotics Research*, vol. 30, no. 13, pp. 1585–1595, 2011.

[15] G. van Oort, R. Carloni, D. Borgerink, and S. Stramigioli,

"An energy efficient knee locking mechanism for a dynamically walking robot," in *Robotics and Automation (ICRA), 2011 IEEE International Conference on*, May 2011, pp. 2003–2008.

[16] M. Plooij and M. Wisse, "A novel spring mechanism to reduce energy consumption of robotic arms," in *Intelligent Robots and Systems (IROS), 2012 IEEE/RSJ International Conference on*, Oct 2012, pp. 2901–2908.

[17] D. F. B. Haeufle, M. D. Taylor, S. Schmitt, and H. Geyer, "A clutched parallel elastic actuator concept: Towards energy efficient powered legs in prosthetics and robotics," in *Biomedical Robotics and Biomechatronics (BioRob), 2012 4th IEEE RAS EMBS International Conference on*, June 2012, pp. 1614–1619.

[18] M. Khoramshahi, A. Parsa, A. Ijspeert, and M. N. Ahmadabadi, "Natural dynamics modification for energy efficiency: A data-driven parallel compliance design method," in *Proceedings of 2014 IEEE International Conference on Robotics and Automation*, 2014, pp. 2412–2417.

[19] G. Mathijssen, D. Lefeber, and B. Vanderborght, "Variable recruitment of parallel elastic elements: Series–parallel elastic actuators (spea) with dephased mutilated gears," *Mechatronics, IEEE/ASME Transactions on*, vol. PP, no. 99, pp. 1–9, 2014.

[20] J. Realmuto, G. Klute, and S. Devasia, "Nonlinear passive cam-based springs for powered ankle prostheses," *Journal of Medical Devices*, vol. 9, no. 1, p. 011007, 2015.

[21] G. Pratt and M. Williamson, "Series elastic actuators," in *Intelligent Robots and Systems 95. 'Human Robot Interaction and Cooperative Robots', Proceedings. 1995 IEEE/RSJ International Conference on*, vol. 1, Aug 1995, pp. 399–406 vol.1.

[22] J. E. Pratt and B. T. Krupp, "Series elastic actuators for legged robots," in *Defense and Security*. International Society for Optics and Photonics, 2004, pp. 135–144.

[23] R. Ham, T. Sugar, B. Vanderborght, K. Hollander, and D. Lefeber, "Compliant actuator designs," *Robotics Automation Magazine, IEEE*, vol. 16, no. 3, pp. 81–94, September 2009.

[24] J. Hurst, "An actuator with mechanically adjustable series compliance," 2004.

[25] B. Vanderborght, A. Albu-Schaeffer, A. Bicchi, E. Burdet, D. Caldwell, R. Carloni, M. Catalano, O. Eiberger, W. Friedl, G. Ganesh, M. Garabini, M. Grebenstein, G. Grioli, S. Haddadin, H. Hoppner, A. Jafari, M. Laffranchi, D. Lefeber, F. Petit, S. Stramigioli, N. Tsagarakis, M. V. Damme, R. V. Ham, L. Visser, and S. Wolf, "Variable impedance actuators: A review," *Robotics and Autonomous Systems*, vol. 61, no. 12, pp. 1601 – 1614, 2013.

[26] L. Chen, M. Garabini, M. Laffranchi, N. Kashiri, N. G. Tsagarakis, A. Bicchi, and D. G. Caldwell, "Optimal control for maximizing velocity of the compact compliant actuator," in *Robotics and Automation (ICRA), IEEE International Conference on*, May 2013, pp. 516–522.

[27] E. J. Rouse, L. M. Mooney, E. C. Martinez-Villalpando, and H. M. Herr, "Clutchable series-elastic actuator: Design of a robotic knee prosthesis for minimum energy consumption," in *Rehabilitation Robotics (ICORR), IEEE International Conference on*, June 2013, pp. 1–6.

[28] G. Mathijssen, R. Furnemont, S. Beckers, T. Verstraten, D. Lefeber, and B. Vanderborght, "Cylindrical cam mechanism for unlimited subsequent spring recruitment in series-parallel elastic actuators," in *Robotics and Automation (ICRA), 2015 IEEE International Conference on*, May 2015, pp. 857–862.

[29] S. Stramigioli, G. van Oort, and E. Dertien, "A concept for a new energy efficient actuator," in *Advanced Intelligent Mechatronics, 2008. AIM 2008. IEEE/ASME International Conference on*, July 2008, pp. 671–675.

[30] S. Au *et al.*, "Powered ankle-foot prosthesis for the improvement of amputee ambulation," in *Engineering in Medicine and Biology Society (EMBS), 29th Annual International Conference of the IEEE*, Aug 2007, pp. 3020–3026.

[31] M. Eslamy *et al.*, "Effects of unidirectional parallel springs on required peak power and energy in powered prosthetic ankles: Comparison between different active actuation concepts," in *Robotics and Biomimetics (ROBIO), IEEE International Conference on*, Dec 2012, pp. 2406–2412.

[32] M. Plooij, M. Van Nunspeet, M. Wisse, and H. Vallery, "Design of the bi-directional clutched parallel elastic actuator (bic-pea)," in *Robotics and Automation (ICRA), 2015 IEEE International Conference on*, 2015.

[33] M. Plooij, G. Mathijssen, P. Cherelle, D. Lefeber, and B. Vanderborght, "Lock your robot: A review of locking devices in robotics," *Robotics Automation Magazine, IEEE*, vol. 22, no. 1, pp. 106–117, March 2015.

[34] W. Roozing, Z. Li, G. A. Medrano-Cerda, D. G. Caldwell, and N. G. Tsagarakis, "Development and control of a compliant asymmetric antagonistic actuator for energy efficient mobility," *IEEE/ASME Transactions on Mechatronics*, vol. 21, no. 2, pp. 1080–1091, April 2016.

[35] M. A. Patterson and A. V. Rao, "Gpops- ii: A matlab software for solving multiple-phase optimal control problems using hp–adaptive gaussian quadrature collocation methods and sparse nonlinear programming," *ACM Transactions on Mathematical Software*, vol. 39, no. 3, pp. 1–41, 2013.

[36] M. Plooij, T. van der Hoeven, G. Dunning, and M. Wisse, "Statically balanced brakes," *Precision Engineering*, vol. 43, pp. 468 – 478, 2016.

[37] S. Diller, C. Majidi, and S. H. Collins, "A lightweight, low-power electroadhesive clutch and spring for exoskeleton actuation," in *IEEE International Conference on Robotics and Automation (ICRA)*, May 2016, pp. 682–689.